9-2012

The Effect Of The Charge-separating Interface On Exciton Dynamics In Photocatalytic Colloidal Heteronanocrystals

Timothy O'Connor

Maxim S. Panov

Andrey Mereshchenko

Alexander N. Tarnovsky
Bowling Green State University, atarnov@bgsu.edu

Ryan Lorek

See next page for additional authors

The Effect of the Charge-Separating Interface on Exciton Dynamics in Photocatalytic Colloidal Heteronanocrystals

Timothy O'Connor,[§] Maxim S. Panov,[†,‡] Andrey Mereshchenko,[†,‡] Alexander N. Tarnovsky,[†,‡] Ryan Lorek,[§] Dimuthu Perera,[§] Geoffrey Diederich,[§] Scott Lambright,[§] Pavel Moroz,[†,‡] and Mikhail Zamkov[†,§,*]

[†]The Center for Photochemical Sciences, [‡]Department of Chemistry, and [§]Department of Physics, Bowling Green State University, Bowling Green, Ohio 43403, United States

ABSTRACT

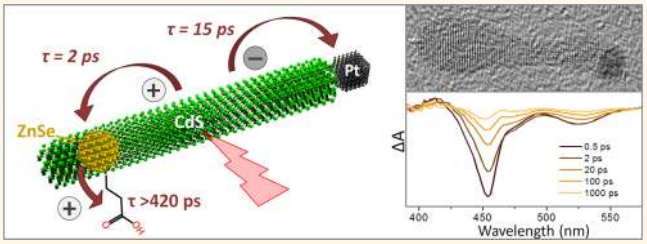

Ultrafast transient absorption spectroscopy was used to investigate the nature of photoinduced charge transfer processes taking place in ZnSe/CdS/Pt colloidal heteronanocrystals. These nanoparticles consist of a dot-in-a-rod semiconductor domain (ZnSe/CdS) coupled to a Pt tip. Together the three components are designed to dissociate an electron–hole pair by pinning the hole in the ZnSe domain while allowing the electron to transfer into the Pt tip. Separated charges can then induce a catalytic reaction, such as the light-driven hydrogen production. Present measurements demonstrate that the internal electron–hole separation is fast and results in the localization of both charges in nonadjacent parts of the nanoparticle. In particular, we show that photoinduced holes become confined within the ZnSe domain in less than 2 ps, while electrons take approximately 15 ps to transition into a Pt tip. More importantly, we demonstrate that the presence of the ZnSe dot within the CdS nanorods plays a key role both in enabling photoinduced separation of charges and in suppressing their backward recombination. The implications of the observed exciton dynamics to photocatalytic function of ZnSe/CdS/Pt heteronanocrystals are discussed.

KEYWORDS: catalysis · photovoltaics · nanorods · dye-sensitized · Schottky · solids · titanium dioxide

Photoinduced charge separation represents an essential step in the process of solar energy conversion through photovoltaic or photocatalytic reactions. An ongoing search for an artificial system exhibiting such charge-separating capabilities has recently identified a promising approach, which relies on the integration of the two semiconductor domains exhibiting complementary donor and acceptor functionalities into a single nanoscale reactor.[1−3] When energetically optimized, the two domains of the resulting composite nanocrystal (NC) can promote fast and near-complete separation of excited charges across donor–acceptor interfaces. Notably, the overall efficiency of charge transfer processes in these composites is facilitated by a direct, "heteroepitaxial" domain coupling as well as the relatively low exciton binding energy in semiconductor nanomaterials. Meanwhile, an all-inorganic composition of heteronanocrystals ensures their compelling stability against the processes of photodecomposition by ultraviolet photons and thermal degradation in heat-intensive applications. Owing to these benefits, several types of donor–acceptor heteronanocrystals comprising CdSe/ZnSe,[1,4] ZnSe/CdS,[5−8] CdSe/CdS,[9−12] CdSe/CdTe,[13−17] and ZnTe/CdSe[18,19] semiconductor combinations have been demonstrated in recent years as potential candidates for solar energy conversion. These studies have also made it clear that the integration of composite nanocrystals into photovoltaic or photocatalytic systems will require the development of novel, often intricate schemes for interfacing both the donor and acceptor components with charge-collecting moieties.

As illustrated by a number of recent reports, the functionality of donor–acceptor heteronanocrystals can be greatly increased if one of the semiconductor components is appended with a metal nanoparticle.[20] Such metal domains, fabricated from small-size gold[21−23] or platinum[24−28] nanocrystals, can serve the role of an electron sink, thus mimicking the action of a photocathode in photocatalytic or photovoltaic processes.

* Address correspondence to zamkovm@bgsu.edu.

Received for review June 25, 2012 and accepted August 10, 2012.

Published online August 11, 2012
10.1021/nn302810y

The success of this methodology was exemplified in a number of experiments, where charge-separating CdSe/CdS[27] or ZnSe/CdS[28] heteronanocrystals were coupled to a small-diameter platinum nanoparticle. The resulting hybrid assemblies were shown to drive an efficient hydrogen production under visible radiation. In these studies, a near-complete charge separation was achieved by using a dot-in-a-rod donor–acceptor morphology, for which electron-donating ZnSe or CdSe semiconductor quantum dots were employed to seed the asymmetric growth of electron-accepting CdS nanorods appended with a Pt tip. Upon absorption of light, the resulting three-domain system promoted the dissociation of excitons by driving the photoinduced electrons into the Pt domain, while forcing the photogenerated holes to localize within the ZnSe (CdSe) dot. The photocatalytic cycle was completed when both an electron and a hole exited the heteronanocrystal through the processes of proton reduction ($2H^+ + 2e \rightarrow H_2$) and oxidation of the sacrificial agent (*e.g.*, $CH_3OH + 2\,h \rightarrow CH_2O + 2H^+$), respectively. Notably, despite the multistep nature of this reaction, the efficiency of H_2 generation was primarily dependent on the rate of the initial electron–hole separation, which placed both charges in a long-lived charge separated state, thus allowing carriers to perform their respective catalytic functions.

Here we employ ultrafast transient absorption spectroscopy to probe the exciton dynamics in photocatalytic ZnSe/CdS/Pt colloidal heteronanocrystals. The experimental data confirms a fast dissociation of electron–hole pairs in these nanoparticles, which leads to the localization of both charges in nonadjacent parts of the structure. By comparing the measured charge transfer rates with that of a CdS/Pt system, we demonstrate that the presence of the ZnSe/CdS charge-separating interface facilitates the spatial separation of photoinduced charges and is critical for suppressing their backward recombination. In particular, we show that photoinduced holes become confined within the ZnSe domain in less than 2 ps, while electrons take approximately 15 ps to transition into a Pt tip. Immediately following the charge separation in ZnSe/CdS/Pt heteronanocrystals, Pt-localized electrons become available for a catalytic reaction, while photoinduced holes still need to be advanced to the surface of the nanocrystal for a sacrificial regeneration. In this study we employ fluorescence intensity decay measurements to estimate the hole activation time to be greater than 420 ps. The implications of the observed exciton dynamics to photocatalytic function of ZnSe/CdS/Pt heteronanocrystals are discussed.

RESULTS AND DISCUSSION

A detailed description of the three-step procedure involved in the preparation of ZnSe/CdS/Pt colloidal heteronanocrystals has been reported previously[28]

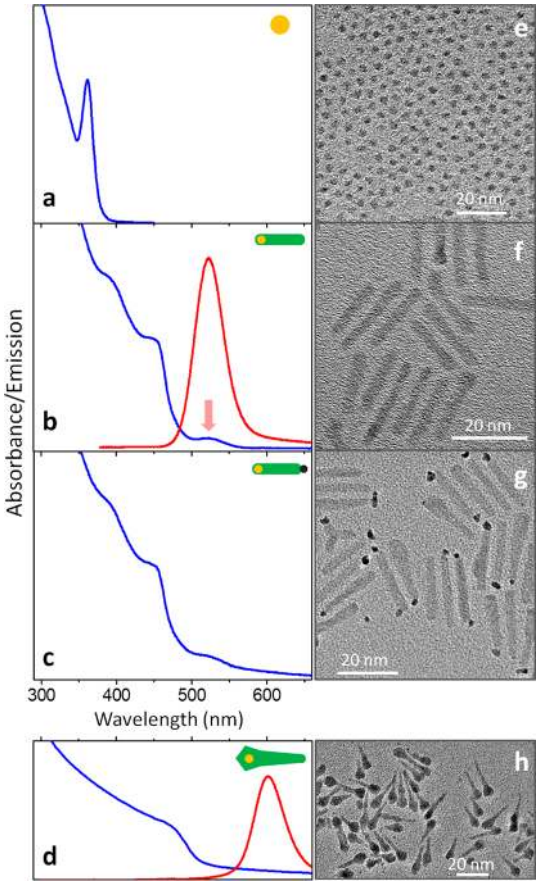

Figure 1. Steady state absorption and emission spectra (a–d) of nanoparticles fabricated at intermediate stages during the three-step synthesis of ZnSe/CdS/Pt heteronanocrystals. (a) ZnSe NCs; (b) ZnSe/CdS nanorods grown from ZnSe NC seeds; (c) ZnSe/CdS nanorods after deposition of the Pt catalyst; (d) ZnSe/CdS nanorods grown from large-diameter ZnSe/CdS core shell NC seeds. The corresponding TEM images (e–h) are shown in the right panel of the figure.

and is provided in the Experimental Section. In brief, small-diameter ZnSe NCs, prepared using hot-injection routes[54] were overcoated with a thin shell of CdS (*ca.* 1–3 monolayers). The resulting ZnSe/CdS core/shell heterostructures (or "bare" ZnSe NCs) were then used as nanoparticle seeds for nucleating the growth of CdS nanorods. The length and the thickness of ZnSe/CdS nanorods were controlled by tuning the amount and the diameter of ZnSe/CdS seeds, respectively. In the final step, Pt tips were grown preferentially onto one of the CdS facets using a methodology reported in ref 29.

Figure 1 shows steady-state optical spectra (a–d) and characteristic transmission electron microscope (TEM) images (e–h) of fabricated heteronanocrystals corresponding to the successive stages of the ZnSe/CdS/Pt growth protocol. ZnSe NCs, fabricated in the first step of the procedure (Figure 1e), were 2.7 nm in diameter with a typical size dispersion of 7%. To initiate the growth of CdS nanorods, either "bare" ZnSe or core/shell ZnSe/CdS NCs (Supporting Information, Figure SF1) were used as nanoparticle seeds. The effect

of an intermediate CdS shell on the ultimate shape of ZnSe/CdS nanorods can be seen through the comparison of Figure 1 panels h and f. Growth of the CdS nanorods from uncoated ZnSe seeds results in cylindrical ZnSe/CdS structures with a narrow diameter (d < 4.5 nm). Conversely, when nanorods are nucleated at large-diameter ZnSe/CdS core/shell NCs, the resulting heterostructures are tapered from the location of the original seed (see Figure 1h). The average length of grown nanorods used in the spectroscopic measurements was 25.5 nm, with a standard length dispersion of 11%. Lastly, the deposition of Pt onto ZnSe/CdS heteronanocrystals resulted in the growth of *ca.* 2.2−2.9-nm metal tips (Figure 1g), forming primarily on one side of the nanorods. Such anisotropic growth of Pt was first demonstrated by Mokari *et al.*[29] and was attributed to the fact that the wurtzite crystalline structure of CdS leads to uneven rates of Pt nucleation on Cd- and S-rich nanorod facets. The elemental composition and crystallographic structure of ZnSe/CdS/Pt heteronanocrystals was analyzed using energy dispersive X-ray and X-ray powder diffraction methods, respectively (see Supporting Information, Figure SF2).

The character of electron−hole localization in fabricated heteronanocrystals was substantiated based on their respective optical properties. For ZnSe NCs dispersed in chloroform, the absorption spectrum contained a sharp excitonic feature around λ = 360 nm, corresponding to the lowest energy $1S(e)-1S_{3/2}(h)$ transitions in these nanoparticles. No band gap emission was detected in this case. The subsequent growth of CdS nanorods nucleated at ZnSe seeds was accompanied by the onset of a strong absorbing transition at the CdS band edge ($\lambda \approx$ 455 nm) along with a smaller feature centered at λ = 525 nm. The origin of the latter peak is attributed to a "spatially-indirect" recombination of carriers, $1S_e(CdS) \leftrightarrow 1S_h(ZnSe)$, a process commonly observed in type II semiconductor heteronanocrystals.[7,8,30] The spectral position of this feature (marked with a red arrow in Figure 1b) is in good agreement with the "spatially-indirect" emission peak in ZnSe/CdS nanorods (red curve), which is red-shifted by only a few nanometers from its corresponding absorbing transition (a relative alignment of electron and hole energies in ZnSe/CdS nanorods is illustrated in Supporting Information, Figure SF5). The interdomain (CdS(e) → ZnSe(h)) character of the "spatially-indirect" emission in ZnSe/CdS nanorods was likewise manifested by the relatively low energy of corresponding photons, which falls below the band gap of both CdS and ZnSe semiconductor domains. Further support of the interdomain carrier recombination in ZnSe/CdS nanorods is provided by the enhanced FL lifetime of the $1S_e(CdS) \rightarrow 1S_h(ZnSe)$ emission band (τ = 75 ns, see Supporting Information, Figure SF3), which exceeds the typical lifetime values of binary semiconductor nanocrystals (e.g., τ (CdSe) < 15 ns).[31] This is attributed to a weak spatial overlap of carriers residing in ZnSe and CdS domains.

The temporal dynamics of excited charge carriers in ZnSe/CdS/Pt heteronanocrystals was investigated using femtosecond transient absorption (TA) spectroscopy. This approach is rapidly becoming the method of choice for decoding ultrafast behavior of excitons in semiconductor heteronanocrystals owing to its competitive temporal resolution and the straightforward correspondence of the observed spectral (bleach) dynamics with electronic transitions in nanocrystals. In recent years both femtosecond and picosecond TA pump−probe spectroscopy have been used to measure the rates of exciton dissociation in a number of donor−acceptor heteronanocrystals, including CdSe/CdTe,[32−36] CdSe/CdS,[37,38] ZnSe/CdS,[6,55,39] CdSe/ZnTe,[40] and CdTe/CdS[41] systems. The primary outcome of these investigations was the demonstration of a fast photoinduced charge transfer across semiconductor−semiconductor interfaces with typical transition times ranging from 300 fs to 100 ps. The exact transfer rate was found to be dependent both on the type of the charge carrier and the nature of the donor−acceptor interface. Despite a wealth of experimental reports on ultrafast electron phenomena in semiconductor nanocrystals, to date, there have been no experimental accounts on the charge transfer dynamics in donor−acceptor heteronanocrystals appended with catalytically active domains, such as Pt nanoparticles. Moreover, there is some controversy regarding the effect of a metal tip on charge carrier dynamics in a single-phase semiconductor. For instance, it has been reported that metal-semiconductor colloids can trap both photoinduced charges at hybrid interfaces, such as in the case of CdS nanorods capped with large-diameter Au domains,[42] exhibit a very slow semiconductor to metal carrier injection as was reported in the case of ultralong nanorods,[43] or form a long-lived charge separated state.[44]

The structure of ZnSe/CdS/Pt heteronanocrystals selected for this study was chosen to be similar to the morphology of photocatalytically active nanocomposites reported earlier.[27,28] Specifically, the size of the Pt domain was kept below 3 nm to suppress the unwanted trapping of photoinduced charges at metal−semiconductor interfaces. Such small-diameter Pt tips were previously shown to drive an efficient generation of H_2 by CdS/Pt composites with an associated quantum yield of up to 4%.[26] To better understand the unique role of each of the three domains (ZnSe, CdS, Pt) participating in the charge-separating process, TA measurements were performed on four types of heterostructures including CdS nanorods, ZnSe/CdS dot-in-a-rod structures, Pt-tipped CdS, and Pt-tipped ZnSe/CdS heteronanocrystals. To suppress the spectral distortions of TA traces associated with the Stark effect,[45,46] relatively low excitation intensities, corresponding to the

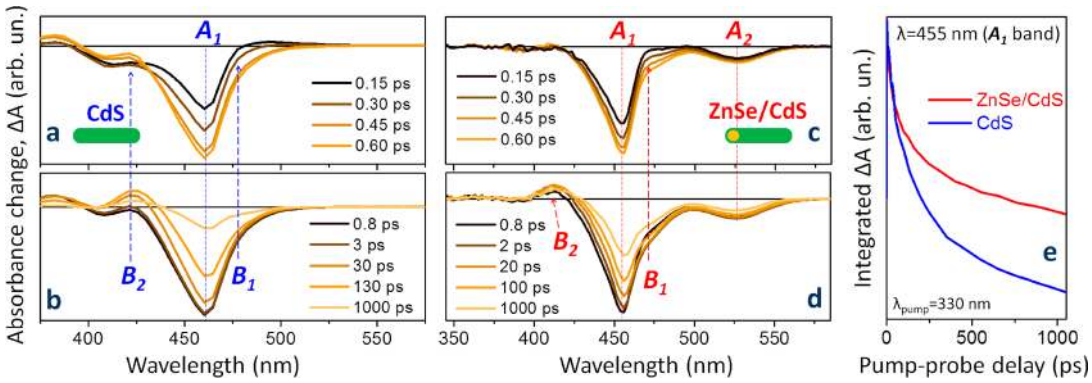

Figure 2. Comparison of the transient absorption spectra of all-CdS (a,b) and ZnSe-seeded CdS (c,d) nanorods. The wavelength of the pump beam was set to 330 nm. Both structures exhibit a strong TA bleach at λ = 455 nm corresponding to the $1S_{3/2}(h) \rightarrow 1S(e)$ transition in CdS (labeled as A_1), as well as small-amplitude photoinduced absorption features labeled B_1 and B_2 (see text). The TA spectra of ZnSe/CdS heteronanocrystals contain the second bleach feature (A_2) attributed to the spatially indirect absorption, $1S_h(ZnSe) \rightarrow 1S_e(CdS)$. (e) The temporal evolution of the $1S_{3/2}(h)1S(e)$ bleach for the all-CdS and ZnSe/CdS nanostructures.

linear power dependence regime were used ($P < 1.5\ \mu$J per pulse, beam diameter $\approx 300\ \mu$m). We also note that the contribution of photoinduced electrons into the observed transient absorption spectra is expected to be greater than that of holes[47] due to comparatively low effective masses of positive charges in bulk CdS,[48,49] as well as the high degeneracy of hole states in CdS NCs.

First, we investigate the charge carrier dynamics in all-semiconductor CdS heterostructures fabricated with and without the use of ZnSe NC seeds. Figure 2 shows the two sets of chirp-corrected transient absorption spectra resulting from the UV excitation (λ = 330 nm) of CdS (Figure 2a,b) and ZnSe/CdS (Figure 2c,d) nanorods. A strong TA bleach (labeled as A_1) near $\lambda \approx 455$ nm, observed for both structures, was attributed to the excitation-induced state filling of the lowest-energy $1S(e)-1S_{3/2}(h)$ transitions in the CdS domain. In addition to A_1, both structures contain derivative-like spectral distortions labeled as B_1 and B_2. The former feature, B_1, is seen as a superposition of the A_1 negative bleach with a positive transient absorption shoulder. This excitation is relatively short-lived ($\tau < 0.6$ ps for both CdS and ZnSe/CdS) and was previously attributed to the effect of hot excitons, whose presence shifts the $1S(e)1S_{3/2}(h)$ exciton band to lower energy.[50] The B_2 feature has a lifetime comparable to that of A_1 and reflects the interaction of $1S(e)1S_{3/2}(h)$ excitons with other exciton bands.[51] Finally, the TA spectrum of ZnSe/CdS contains an additional bleach signal labeled as A_2. This feature is not present in pure CdS structures, and is attributed to the $1S_h(ZnSe) \rightarrow 1S_e(CdS)$ spatially indirect absorbing transitions in ZnSe/CdS nanorods.

A comparison of the exciton dynamics for the $1S(e)-1S_{3/2}(h)$ band (labeled A_1) between CdS and ZnSe/CdS heterostructures (Figure 2) indicates that the excited state population tends to deplete quicker in CdS nanorods. Indeed, the half-life of the bleach in CdS nanorods is approximately 180 ps, while for ZnSe/CdS nanoparticles the recovery of the same transition takes over 1000 ps. A possible cause of this difference can be linked to the existence of the charge separating interface in ZnSe/CdS heteronanocrystals, which reduces the spatial overlap between electrons and holes. A less extensive overlap gives rise to a slower recombination of carriers in these nanoparticles resulting in a delayed bleach recovery. It could be argued that trapping of photoinduced holes on dangling bonds of all-CdS nanorods can provide a similar type of hole localization as does the ZnSe domain in ZnSe/CdS NCs. This could potentially cause carriers in both structures to decay with similar rates. However, in the case of ZnSe/CdS heteronanocrystals, electrons are forced away from the hole localization site by the interfacial offset of the potential energy. Meanwhile, in all-CdS nanorods, an electron wave function is delocalized over the entire structure, and thus can have a significant overlap with a trapped hole.

Further evidence supporting a correlation between the slower recovery of $1S(e)1S_{3/2}(h)$ excitons in ZnSe/CdS nanorods and the existence of a charge-separating interface (ZnSe/CdS) is provided by the dynamics of B_1 bleach. As was demonstrated previously, the onset of the B_1 feature at longer pump–probe times ($10\text{ ps} < \tau < 1000$ ps) can be attributed to the existence of a long-lived charge separated state.[44] In CdS nanorods, the B_1 feature disappears within 0.6 ps and is absent for the rest of the observation time window. For ZnSe/CdS heteronanocrystals, a weak B_1 feature reappears after $\tau > 20$ ps (see Supporting Information, Figure SF4), as a clear modification of the red-shifted half of the A_1 bleach signal. This points toward the presence of a charge-separated state, whose electric field perturbs $1S(e)1S_{3/2}(h)$ excitons causing the onset of B_1. On the basis of these observations we conclude that longer recovery times in ZnSe/CdS NCs is likely the effect of an enhanced electron–hole separation in these nanoparticles as compared to CdS nanorods.

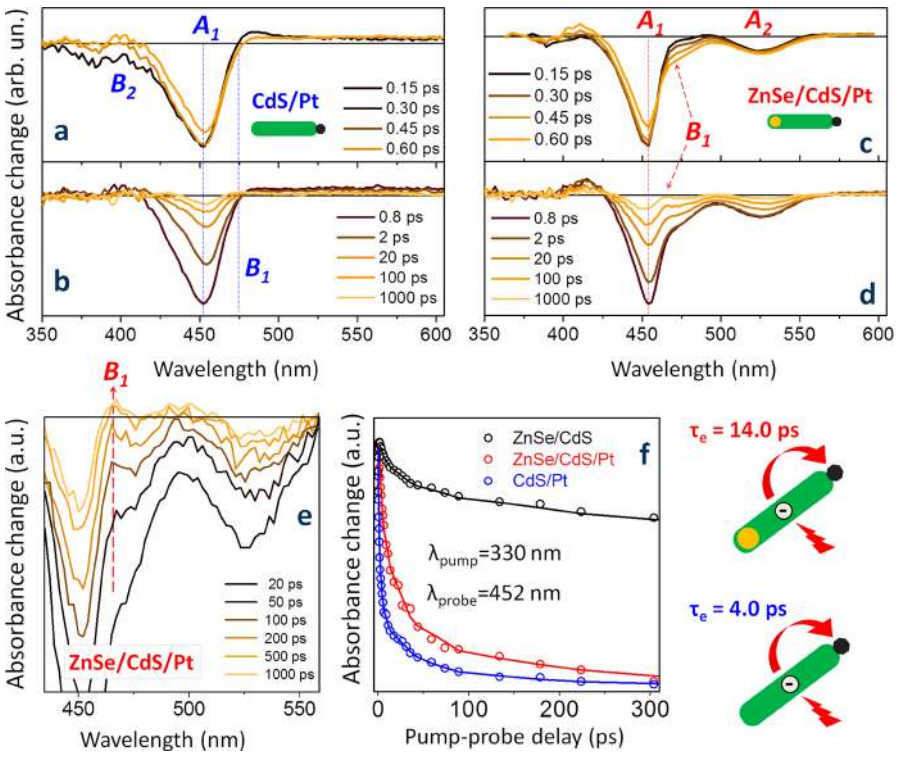

Figure 3. Transient absorption spectra of Pt-tipped nanorods: (a,b) CdS/Pt and (c,d) ZnSe/CdS/Pt. The wavelength of the pump beam was set to 330 nm. Both structures exhibit a TA bleach at λ = 455 nm corresponding to the $1S_{3/2}(h) \rightarrow 1S(e)$ transition in CdS (A_1), as well as smaller-amplitude photoinduced absorption features (B_1 and B_2). (e) Transient absorption spectra of ZnSe/CdS/Pt heteronanocrystals showing the onset of B_1 feature, reflecting the formation of the spatially separated electron−hole pair. (f) The temporal evolution of the $1S_{3/2}(h)1S(e)$ bleach for ZnSe/CdS (black), ZnSe/CdS (black), and ZnSe/CdS/Pt (red), and CdS/Pt (blue) nanostructures.

The ultrafast dynamics of CdS/Pt and ZnSe/CdS/Pt heteronanocrystals containing a Pt tip is analyzed in Figure 3. We first consider the TA dynamics of CdS/Pt structures excited at λ_{exc} = 330 nm. According to Figure 3, the spectra of CdS/Pt nanoparticles exhibit all three TA features found in all-CdS nanorods: A_1, B_1, and B_2 (Figure 3a,b), but the recovery of these excitations in now modified by the presence of the Pt tip. The most evident distinction between the decay dynamics of CdS and CdS/Pt structures is the difference in the rate of A_1 recovery. Notably, the half-life of $1S(e)1S_{3/2}(h)$ excitons in CdS is 180 ps, while in Pt-tipped CdS structures, the A_1 bleach recovers in just 3.1 ps (Figure 3f). This dramatic increase in the decay rate reflects the transfer of excited electrons (and possibly holes) from the CdS domain into the Pt tip[43,44] (or Pt islands that tend to form along the surface of CdS) as was previously observed for CdS/Pt heteronanocrystals. Such charge transfer mechanism is consistent with a significant driving force for both carriers in CdS to fill the Fermi level states of Pt, and is often manifested through the effect of the fluorescence suppression in metal tipped semiconductors.[52] It should be noted that the transfer of photoinduced holes into a metal tip could also play a role in depleting the excited state population, as can be inferred from the negative energy of the 1S(h) state with respect to the Pt Fermi level. However, this process does not contribute equally to the TA bleach signal and thus cannot be distinguished from the dominant electron transfer contribution.

The increased rate of exciton dissociation caused by the presence of a Pt domain was also observed in the case of ZnSe/CdS/Pt heteronanocrystals (Figure 3c, d). For ZnSe-seeded structures, the recovery of the band gap bleach in the CdS domain (A_1) occurred within 15 ps (Figure 3f), which is substantially faster than the recovery of the corresponding bleach signal in bare ZnSe/CdS nanorods (τ > 1000 ps). Similar to the case of CdS/Pt nanocrystals, the enhanced recovery rate was attributed to the transfer of photoinduced charges into the Pt domain. The transfer of an electron away from the semiconductor component has also caused a faster recovery of the A_2 transition, (τ (A_2) = 35 ps), attributed to the depletion of $1S_e$ population in CdS, and the B_2 feature, which amplitude is proportional to A_1 bleach.

The difference in the exciton dissociation times between CdS/Pt (3.1 ps) and ZnSe/CdS/Pt (15 ps) heteronanocrystals was ascribed to the existence of the charge-separating interface in ZnSe/CdS/Pt nanoparticles. As was demonstrated above, the presence of ZnSe seeds in CdS nanorods affects the subnanosecond carrier dynamics (20 < τ < 1000 ps) in ZnSe/CdS heterostructures manifested as a slower recovery of the A_1 bleach. A similar trend is observed here for

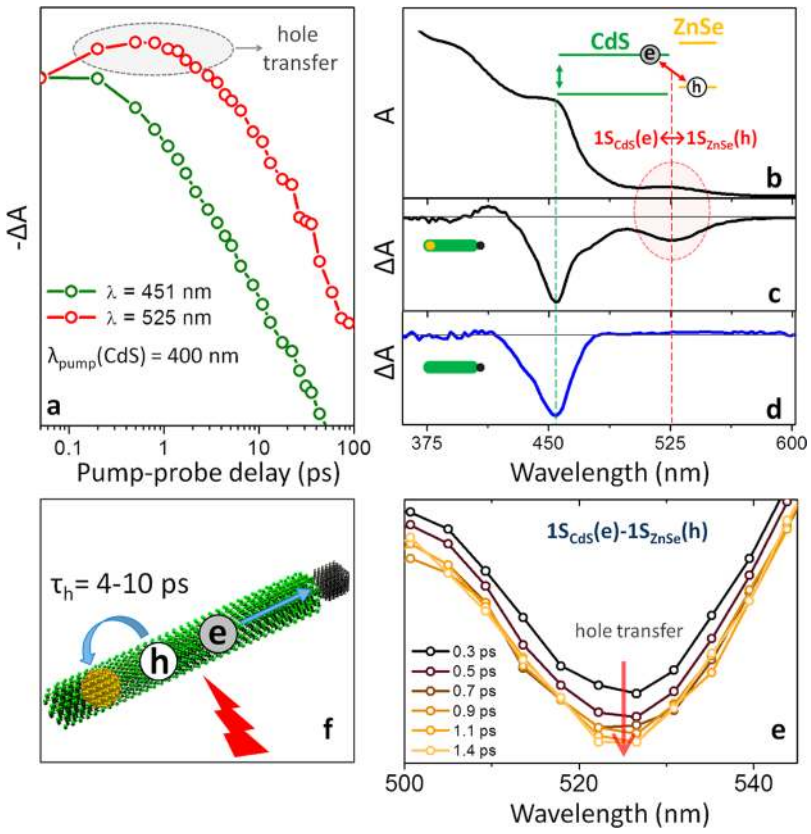

Figure 4. (a) Recovery of the TA bleach for the two spectral bands in ZnSe/CdS/Pt nanorods associated with $1S_h$(CdS) → $1S_e$(CdS) (green curve) and $1S_h$(ZnSe) → $1S_e$(CdS) (red curve) transitions. (b) Steady state absorption spectra of ZnSe/CdS/Pt heteronanocrystals showing the onset of spatially indirect absorbing transition, $1S_h$(ZnSe) → $1S_e$(CdS). (c) TA spectra of ZnSe/CdS/Pt nanorods highlighting the $1S_h$(ZnSe) → $1S_e$(CdS) bleach near λ = 525 nm. (d) TA spectra confirming the lack of the spatially indirect $1S_h$(ZnSe) → $1S_e$(CdS) bleach in single-phase CdS nanorods appended with a Pt tip. (e) Temporal evolution of the TA bleach centered near the $1S_h$(ZnSe) → $1S_e$(CdS) transition. The early time increase in the bleach strength is attributed to a hole transfer from CdS into ZnSe (see text). (f) Schematic representation of the hole transfer process in ZnSe/CdS/Pt heteronanocrystals.

Pt-tipped heteronanocrystals on a picosecond time scale. The presence of the ZnSe seed within a CdS rod results in a slower transfer of photoinduced electrons from CdS into Pt. This could be attributed to the electron–hole attraction. Indeed, it is expected that the electron–hole interaction in ZnSe/CdS/Pt structures will cause the electron density to increase near the ZnSe domain (where the hole is localized) and to consequently decrease at the tip of the nanorod. As a result, an overlap between excited electron wave functions and conduction states of the Pt nanoparticle will be smaller for ZnSe/CdS/Pt heteronanocrystals, leading to a slower transfer. We note that in all-CdS structures, a trapped hole can also enhance the electron density near its location. However, in this case, the location of the hole may likely be near the Pt tip, where most traps are being produced due to Pt deposition. This would result in enhanced electron density near the tip, and consequently faster electron transfer into Pt, as seen in Figure 3f.

An important role of the ZnSe/CdS interface in the charge-separation dynamics of Pt-tipped nanorods is further exemplified by the temporal evolution of the B_1 photoinduced absorption (PA) feature. As stated above, the onset of B_1 at longer pump–probe delay ($\tau > 20$ ps) corresponds to the formation of the charge separated state. Here, the B_1 feature is much more prominent in the case of ZnSe-seeded structures (see Figure 3e), indicating a stronger electric dipole associated with an electron–hole pair for these nanoparticles. Consequently, the spatial separation of charges is more extensive when ZnSe seed is present within CdS rods. We note that the extent of spatial charge separation is an important property of photocatalytic structures as it helps suppressing the backward recombination of charges.

To understand the dynamics of photoinduced holes in ZnSe/CdS/Pt heteronanocrystals, we focus on the A_2 feature (λ = 525 nm) that was previously identified as the spatially indirect absorbing transition at the ZnSe/CdS interface[6] involving both electron and hole states (see the insert in Figure 4b). Similar to A_1, the recovery of A_2 bleach is accelerated by the presence of the Pt tip; however, the rate of the recovery is only half that of A_1. To identify electronic processes underlying the decay of A_2, the wavelength of the excitation pulse was set to 400 nm. In this case, the direct excitation of band edge excitons in ZnSe is energetically inaccessible, such that

the only transition contributing into A_2 bleach is the excitation of valence electrons occupying the ZnSe domain into the conduction band of CdS. One can expect that due to the subsequent CdS → Pt electron transfer, these interdomain excitons will be quickly depleted. However, the temporal dynamics of the integrated bleach area shows a distinct rise at early probe times (τ < 2 ps). The delayed enhancement of the $1S_h$(ZnSe)−$1S_e$(CdS) bleach amplitude strongly suggests that the carrier population in one of the involved states, either $1S_h$(ZnSe) or $1S_e$(CdS), is growing for several picoseconds *after* the excitation pulse. Since the $1S_e$ state of CdS cannot be repopulated due to the lack of excited electrons with energies above that of $1S_e$(CdS) (since λ_{pump} = 400 nm), the rise in the population of interdomain excitons was attributed to the energetically accessible transfer of photoinduced holes from $1S_h$(CdS) into $1S_h$(ZnSe) state. Indeed, the transition of holes from CdS into ZnSe domain is exothermic and is expected to produce a delayed repopulation of the ZnSe valence band, which in turn would result in the enhancement of the $1S_h$(ZnSe)−$1S_e$(CdS) bleach amplitude (λ = 525 nm), as shown in Figure 4e. It should be stressed that a contribution of holes into ΔA is less than that of electrons, as expected due to high hole-to-electron effective mass ratios, but it is not zero. For instance, hole-induced bleaching of the above-the-pump-energy transitions has been observed previously in CdSe/CdS heterostructured nanocrystals.[37]

The transient absorption measurements indicate that the internal separation of photoinduced charges across ZnSe/CdS/Pt nanorods occurs in less than 15 ps. Upon completion of this cycle, electrons become localized in the Pt tip and are ready to perform their respective catalytic functions. Photoinduced holes, on the other hand, still remain confined within the ZnSe domain, which is catalytically inactive. Previous works have shown that the energy of the oxidizing hole can be effectively dissipated if it is expelled to the surface of the structures *via* a ligand-to-semiconductor electron transfer.[27,53] In particular, the use of hydrophilic MUA or 3-mercaptopropionic acid (MPA) ligands facilitate the transfer of the hole to the surface where it is picked up by a scavenger, typically methanol.

The average time associated with the ZnSe-to-ligand hole transfer was determined in this study from the measurements of the fluorescence intensity decay of spatially indirect excitons ($1S_e$(CdS) → $1S_h$(ZnSe)) in MUA-capped ZnSe/CdS nanorods. To ensure that quenching of the emission occurs due to the removal of the valence hole from the ZnSe, and not due to the transfer of photoinduced electrons away from the conduction band of CdS, nanorods were not appended with a Pt tip. In this case the FL lifetime, τ_{FL}, is determined primarily by the competition of two processes: a slow-rate radiative decay (Γ_R) and a nonradiative decay,

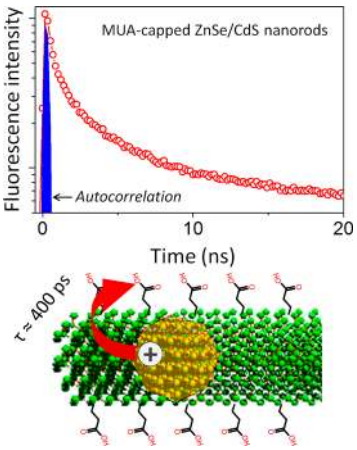

Figure 5. Fluorescence intensity decay of MUA-capped ZnSe/CdS nanorods (red circles) along with the instrument response time (blue curve). The observed FL lifetime of excited carriers is approximately equal to the average time associated with the transfer of holes from ZnSe to MUA.

which includes a slow-rate component associated with charge trapping (Γ_{NR}^{trap}) and a fast-rate component associated with the transfer of holes to surface ligands ($\Gamma_{NR}^{transfer}$). With these considerations, the fluorescence lifetime of the spatially indirect emission of MUA-capped ZnSe/CdS nanorods, τ_{FL}, can be expressed as

$$\tau_{FL} = \tau_R \frac{\Gamma_R}{\Gamma_R + \Gamma_{NR}^{transfer} + \Gamma_{NR}^{trap}} \quad (1)$$

where τ_R is the radiative lifetime of $1S_e$(CdS)$1S_h$(ZnSe) excitons in ZnSe/CdS heteronanocrystals. If we assume that trapping of carriers is slow ($\Gamma_{NR}^{trap} \rightarrow 0$), then the *average* hole transfer time, $\tau_{transfer}$, can be expressed as (see Supporting Information for details):

$$\tau_{transfer} = \tau_{FL}/(1 + (\tau_{FL}/\tau_R)) \quad (2)$$

The equation stipulates that the radiative lifetime of $1S_e$(CdS)$1S_h$(ZnSe) excitons should be known in order to estimate the hole transfer time. Since the FL lifetime of MUA-capped nanorods, τ_{FL} (~400 ps), is much smaller than the corresponding radiative lifetime (>100 ns),[5] a good approximation of τ_R can be derived from the FL lifetime of TOPO-capped nanocrystals. To illustrate this point, we refer to Figure 5 showing the FL intensity decay of MUA-capped ZnSe/CdS nanorods in water. The emission lifetime (τ = 420 ps) in this case is 2 orders of magnitude shorter than the fluorescence lifetime of spatially indirect excitons in TOPO-capped ZnSe/CdS (75 ns, see Supporting Information, Figure SF3). As a result, the average time involved in the transfer of photoinduced holes to the MUA surface ligand is estimated to be $\tau_{transfer} \approx 420 \times (1 + 0.420/75) \approx$ 422.3 ps. If the radiative lifetime happens to be substantially greater than the FL lifetime of TOPO-coated NCs then the actual $\tau_{transfer}$ would become just slightly shorter than 422.3 ps and lie somewhere in the 420−422.3 ps range.

Upon the completion of the hole transfer to the surface ligand, the ZnSe/CdS/Pt system becomes regenerated with both charges exiting the semiconductor portion of the structure. While the ZnSe/CdS domain returns to the ground state in approximately 0.42 ps, the spatial proximity of exited charges may still affect the dynamics of the secondary excitations. In particular, the presence of an electron in a Pt tip may slow down the transfer of an additional electron needed for H_2 production. Likewise, the presence of a positive charge on the nanorods surface is likely to produce electrostatic screening effects, whereby altering the electric field at the ZnSe/CdS interface. Future work will be necessary to understand the effect of stored charges on the carrier dynamics in ZnSe/CdS/Pt heteronanocrystals.

CONCLUSION

Transient absorption spectroscopy was employed to investigate the ultrafast dynamics of photoinduced charges in ZnSe/CdS/Pt heterostructured nanocrystals comprising a charge-separating ZnSe/CdS semiconductor component appended with a Pt catalyst. Experimental data provide an estimate of charge transfer rates associated with several sequential processes involved in the photocatalytic cycle of proton reduction. In particular, we show upon photon absorption, photoinduced electron−hole pairs become spatially separated *via* a transfer of holes to ZnSe ($\tau \approx 2.0$ ps) and subsequently dissociate as a result of photoinduced electron transfer into the Pt domain ($\tau \approx 15$ ps). The study also demonstrates that the presence of the ZnSe dot within CdS nanorods plays an important role in enhancing the spatial separation of charges. Furthermore, a comparative analysis indicates that the localization of holes in the ZnSe dot slows down the "backward" recombination of separated carriers, which is an important prerequisite for improving the efficiency of a catalytic reaction.

EXPERIMENTAL SECTION

Chemicals. Oleylamine (tech., 70%, Aldrich), sulfur (99.999%, Acros), 1-octadecene (ODE, tech., 90%, Aldrich), cadmium oxide (CdO, 99.99%, Aldrich), octadecylamine (ODA, 90%, Fisher), oleic acid (OA, tech., 90%, Aldrich), tri-*n*-octylphosphine (TOP, 97%, Strem), tri-*n*-octylphosphine oxide (TOPO, 99%, Aldrich), *n*-octadecylphosphonic acid (ODPA, 98%, PCI Synthesis), *n*-hexylphosphonic acid (HPA, 98%, PCI Synthesis), hexadecylamine (HDA, tech, Fluke), 1,2-hexadecane diol (TCI), 11-mercaptoundecanoic acid (MUA, 95%, Aldrich), platinum(II) acetylacetonate (97%, Aldrich), tellurium powder (Te, -200 mesh, 99.8%, Aldrich), diethylzinc (Et_2Zn, 15% wt, 1.1 M solution in toluene, Aldrich), selenium powder (Se, 200 mesh, Acros), hexane (anhydrous, 95%, Aldrich), methanol (anhydrous, 99.8%, Aldrich), ethanol (anhydrous, 95%, Aldrich), *tert*-butanol (99.7%, Aldrich), and toluene (anhydrous, 99.8%, Aldrich) were used as purchased. All reactions were performed under argon atmosphere using the standard air-free Schlenk technique unless otherwise stated. CdS nanorods (NRs) were synthesized using a seeded-type approach by introducing small-diameter seed nanocrystals (NCs) into the reaction mixture for nucleating the growth of CdS extensions.

ZnSe NCs. ZnSe NCs for seeding the growth of CdS nanorods were synthesized according to the procedure reported by Cozzoli *et al.*[54] Briefly, 7.0 g of ODA was degassed at 130 °C with stirring for 90 min in a three-neck flask. After degassing, the solution was switched to argon and heated to 300 °C. (It is important to use a wide exhaust vent as ODA vapors will resolidify at room temperature and clog narrow vents). At this point, a selenium precursor prepared by dissolving 0.063 g of Se in 2.4 mL of TOP through sonication under argon was injected into the reaction flask containing degassed ODA. The mixture was then reheated to 300 °C. To initiate the NC growth, 1.0 mL of a 10% diethyl zinc solution (10% by wt in hexane) was injected directly into the reaction flask and the temperature was allowed to stabilize at 265 °C and was kept at this level for the duration of the reaction. The growth was stopped in approximately 5 min when the position of the absorbance edge in the growing nanocrystals stopped red-shifting and "saturated" near λ = 360 nm. Prolonged growth of nanocrystals sometimes resulted in the formation of nanorods, which was not the desired morphology for ZnSe. After the growth stage, the flask was cooled down to 60 °C, 20 mL of methanol was added, and the flask was reheated back to 60 °C. For the initial cleaning the mixture must be kept at above 55 °C prior to centrifuging to prevent the ODA from solidifying. NCs were precipitated with methanol and redispersed in chloroform twice and stored in chloroform.

Synthesis of ZnSe/CdS Core/Shell. For the growth of CdS shells onto ZnSe seeds, a Cd precursor solution was prepared by dissolving 0.03 g of CdO, 0.6 mL of OA, and 5.4 mL of ODE at 290 °C under argon while stirring. Once a clear solution was obtained, the mixture was allowed to cool to room temperature. Similarly, a sulfur solution was prepared by heating 0.0077 g of sulfur in 6.0 mL of ODE to 200 °C under argon while stirring until clear and cooling to room temperature. In a 3-neck flask, 1.5 g of ODA and 6.3 mL of ODE were combined and degassed at 120 °C for 30 min. After the flask was switched to argon, 1 mL of ZnSe NC solution in chloroform, prepared in the first stage of the procedure, was added into the mixture, and the temperature was raised to 240 °C. The concentration of ZnSe seeds for the shell growth procedure was determined by setting the absorbance of the NC solution at the exciton shoulder ($\lambda \approx 360$ nm) to 1.5 (as measured using a 1-mm-thick cuvette)— approximately half the amount of NCs fabricated in the first stage. Once the temperature of the reaction mixture reached 240 °C, 0.15 mL of the combined mixture of Cd and S precursor solutions was injected every 10 min. The growth of the CdS shell was monitored by measuring the NC emission. For instance, after the second injection, low-intensity red emission appeared due to CdS trap states. The continuous addition of precursors subsequently resulted in the onset of band gap emission at $\lambda \approx 450$ nm, and after 90 min, strong green emission ($\lambda \approx$ 510−520 nm) was observed, at which point the reaction was stopped by raising the flask from the heating mantle. When the solution temperature reached 50 °C, 18 mL of ethanol was added to the flask and the solution was centrifuged to precipitate NCs, which were then redissolved in chloroform. After cleaning the NCs one more time, the precipitate was dissolved in chloroform and stored.

Synthesis of CdS Nanorods using ZnSe/CdS or ZnSe Nanocrystal Seeds. Synthesis of heterostructured nanorods was carried out using a seeded-type growth, according to ref 10. In a typical procedure, 0.120 g of S was dissolved in 1.81 mL of TOP at 200 °C and, after being cooled to room temperature, was mixed with 1 mL of nanocrystal seed solution in TOP. The amount of ZnSe/CdS or ZnSe seeds for the nanorods growth step was determined by setting the absorbance of the NC solution at the excitonic peak to 1.0 (as measured using a 1-mm-thick cuvette). Separately, a mixture of 0.060 g of CdO, 3.0 g of TOPO, 0.290 g of ODPA, and 0.080 g of HPA in a 50 mL 3-neck flask was exposed to vacuum at

150 °C for 30 min. Subsequently, the system was switched to Ar flow and heated to 300 °C until the solution turned optically clear and colorless. At this point, 1.81 mL of TOP was added to the flask and the temperature was raised to 380 °C. The growth of nanorods was initiated with a swift injection of the nanocrystal seeds/sulfur mixture at 380 °C. After the temperature recovered to 350 °C, nanorods were allowed to grow for an additional 7−9 min at 350 °C and the reaction was quenched by raising the flask from the mantle. When the temperature of the reaction mixture reached 60 °C, 14 mL of ethanol was added and the contents were centrifuged. The precipitate was subsequently redissolved in 2 mL of hexane and precipitated one more time using 8 mL of ethanol. The final product was stored in chloroform.

Growth of Pt Tips on CdS NRs. Platinum tips were grown onto the CdS NRs using a previously reported protocol.[29] In a typical procedure, 0.2 mL of OA, 0.2 mL of OLAM, 43 mg of 1,2-hexadecanediol, and 10 mL of diphenyl ether were degassed at 80 °C in a three-neck flask for 1 h. Subsequently, the mixture was switched to argon and the temperature was raised to 200 °C, at which point a mixture of heteronanorods (the entire amount fabricated in the previous step) in chloroform and 20 mg of platinum(II) acetylacetonate was injected. The reaction mixture was heated for 5−7 min, until the solution color turned black and the heat was removed from the flask. Pt-tipped nanorods were cleaned two times by precipitating with the methanol/chloroform (10:3) mixture, designed to separate isolated Pt nanoparticles from Pt-tipped nanorods.

Ligand Exchange of Pt Tipped CdS NRs. The original hydrophobic ligands on Pt-tipped nanorods were exchanged with hydrophilic MUA or MPA molecules using a method reported by Costi *et al.*[22] To this end, the solution of nanorods in 10−12 mL of chloroform was mixed with 10 mg of MUA (MPA). Subsequently, 4 mL of KOH solution (0.1 g KOH in 20 mL ultrapure water) was added and the mixture was vigorously shaken until nanorods were transferred into the aqueous phase. The latter was separated and extracted one more time using 2 mL of aqueous KOH. Finally, MUA-capped nanorods were precipitated with 10 mL of methanol and redissolved in 4 mL of ultrapure water.

Characterization. UV−vis absorption and photoluminescence spectra were recorded using a CARY 50 scan spectrophotometer and a Jobin Yvon Fluorolog FL3-11 fluorescence spectrophotometer. High resolution transmission electron microscopy measurements were carried out using JEOL 311UHR operated at 300 kV. Specimens were prepared by depositing a drop of nanoparticle solution in organic solvent onto a carbon-coated copper grid and allowing it to dry in air. X-ray powder diffraction (XRD) measurements were carried out on a Scintag XDS-2000 X-ray powder diffractometer. FL lifetime measurements were performed using a time-correlated single photon counting setup utilizing SPC-630 single-photon counting PCI card (Becker & Hickle GmbH), picosecond diode laser operating at 400 nm, as an excitation source (Picoquant), and an id50 avalanche photodiode (Quantique).

Transient Absorption Spectroscopy. The laser system for transient absorption measurements was described in earlier reports.[55] The setup was based on a Ti:sapphire amplified laser system (Hurricane, Spectra Physics) operating at a repetition rate of 1 kHz/90-fs (fwhm) and delivering 800-nm laser pulses. The laser output was split into two components: one was directed to the TOPAS-C optical parametric amplifier to produce excitation pulses (120 fs @400 nm), and the second was focused onto a CaF_2 plate to generate a white-light-continuum for broad-band probe pulses (350−800 nm). All transient absorption data were corrected for the group velocity dispersion of the white-light continuum with an accuracy ±25 fs by using the nonresonant ΔA signals from the neat solvent. The incident excitation pulse was attenuated before the sample position using appropriate neutral density filters to ensure the absence of solvent contribution due to nonlinear pump absorption at time delays equal to or longer than $\Delta\tau$ = 500 fs. Linearity of the ΔA was verified by plotting the integrated bleach signal versus excitation pulse energy (400 nm pump, 0.4−4 μJ range, $A = \sim 0.4$ at excitation wavelength).

Conflict of Interest: The authors declare no competing financial interest.

Acknowledgment. We gratefully acknowledge OBOR "Material Networks" program and NSF Award CHE-1112227 for financial support.

Supporting Information Available: X-ray power diffraction data (XRD); additional TEM images and TA spectra. This material is available free of charge *via* the Internet at http://pubs.acs.org.

REFERENCES AND NOTES

1. Donega, C. D. Synthesis and Properties of Colloidal Heteronanocrystals. *Chem. Soc. Rev.* **2011**, *40*, 1512–1546.
2. Carbone, L.; Cozzoli, P. D. Colloidal Heterostructured Nanocrystals: Synthesis and Growth Mechanisms. *Nano Today.* **2010**, *5*, 449–493.
3. Lo, S. S.; Mirkovic, T.; Chuang, C. H.; Burda, C.; Scholes, G. D. Emergent Properties Resulting from Type-II Band Alignment in Semiconductor Nanoheterostructures. *Adv. Mater.* **2011**, *23*, 180–197.
4. Ivanov, S. A.; Nanda, J.; Piryatinski, A.; Achermann, M.; Balet, L. P.; Bezel, I. V.; Anikeeva, P. O.; Tretiak, S.; Klimov, V. I. Light Amplification Using Inverted Core/Shell Nanocrystals: Towards Lasing in the Single-Exciton Regime. *Phys. Chem. B* **2004**, *108*, 10625–10630.
5. Dorfs, D.; Salant, A.; Popov, I.; Banin, U. ZnSe Quantum Dots within CdS Nanorods: A Seeded-Growth Type-II System. *Small* **2008**, *4*, 1319–1323.
6. Hewa-Kasakarage, N. N.; Kirsanova, M.; Nemchinov, A.; Schmall, N.; El-Khoury, P. Z.; Tarnovsky, A. N.; Zamkov, M. Radiative Recombination of Spatially Extended Excitons in (ZnSe/CdS)/CdS Heterostructured Nanorods. *J. Am. Chem. Soc.* **2009**, *131*, 1328–1334.
7. Ivanov, S. A.; Piryatinski, A.; Nanda, J.; Tretiak, S.; Zavadil, K. R.; Wallace, W. O.; Werder, D.; Klimov, V. I. Type-II Core/Shell CdS/ZnSe Nanocrystals: Synthesis, Electronic Structures, and Spectroscopic Properties. *J. Am. Chem. Soc.* **2007**, *129*, 11708–11719.
8. Nemchinov, A.; Kirsanova, M.; Hewa-Kasakarage, N. N.; Zamkov, M. Synthesis and Characterization of Type II ZnSe/CdS Core/Shell Nanocrystals. *J. Phys. Chem. C* **2008**, *112*, 9301–9307.
9. Battaglia, D.; Li, J. J.; Wang, Y.; Peng, X. Colloidal Two-Dimensional Systems: CdSe Quantum Shells and Wells. *Angew. Chem.* **2003**, *42*, 5035–5039.
10. Carbone, L.; Nobile, C.; de Giorgi, M.; Sala, F. D.; Morello, G.; Pompa, P.; Hytch, M.; Snoeck, E.; Fiore, A.; Franchini, I. R.; *et al.* Synthesis and Micrometer-Scale Assembly of Colloidal CdSe/CdS Nanorods Prepared by a Seeded Growth Approach. *Nano Lett.* **2007**, *7*, 2942–2950.
11. She, C.; Demortière, A.; Schevchenko, E. V.; Pelton, M. Using Shape To Control Photoluminescence From CdSe/CdS Core/Shell Nanorods. *J. Phys. Chem. Lett.* **2011**, *2*, 1469.
12. Ruberu, T. P. A.; Vela, J. Expanding the One-Dimensional CdS-CdSe Composition Landscape: Axially Anisotropic $CdS_{1-x}Se_x$ Nanorods. *ACS Nano* **2011**, *5*, 5775–5784.
13. Kim, S.; Fisher, B.; Eisler, H. J.; Bawendi, M. Type-II Quantum Dots: CdTe/CdSe(Core/Shell) and CdSe/ZnTe(Core/Shell) Heterostructures. *J. Am. Chem. Soc.* **2003**, *125*, 11466–11467.
14. Halpert, J. E.; Porter, V. J.; Zimmer, J. P.; Bawendi, M. G. Synthesis of CdSe/CdTe Nanobarbells. *J. Am. Chem. Soc.* **2006**, *128*, 12590–12591.
15. Donega, C. M. Formation of Nanoscale Spatially Indirect Excitons: Evolution of the Type-II Optical Character of CdTe/CdSe Heteronanocrystals. *Phys. Rev. B* **2010**, *81*, 165303.
16. Lo, S. S.; Khan, Y.; Jones, M.; Scholes, G. D. Temperature and Solvent Dependence of CdSe/CdTe Heterostructure Nanorod Spectra. *J. Chem. Phys.* **2009**, *131*, 084714.
17. Kumar, S.; Jones, M.; Lo, S. S.; Scholes, G. D. Nanorod Heterostructures Showing Photoinduced Charge Separation. *Small* **2007**, *3*, 1633–1639.
18. Xie, R.; Zhong, X.; Basché, T. Synthesis, Characterization, and Spectroscopy of Type-II Core/Shell Semiconductor Nanocrystals with ZnTe Cores. *Adv. Mater.* **2005**, *17*, 2741–2745.

19. Cheng, C. T.; Chen, C. Y.; Lai, C. W.; Liu, W. H.; Pu, S. C.; Chou, P. T.; Chou, Y. H.; Chiu, H. T. Syntheses and Photophysical Properties of Type-II CdSe/ZnTe/ZnS (core/shell/shell) Quantum Dots. *J. Mater. Chem.* **2005**, *15*, 3409–3414.
20. Costi, R.; Saunders, A. E.; Banin, U. Colloidal Hybrid Nanostructures: A New Type of Functional Materials. *Angew. Chem., Int. Ed.* **2010**, *49*, 4878–4897.
21. Mokari, T.; Rothenberg, E.; Popov, I.; Costi, R.; Banin, U. Selective Growth of Metal Tips onto Semiconductor Quantum Rods and Tetrapods. *Science* **2004**, *304*, 1787–1790.
22. Costi, R.; Saunders, A. E.; Elmalem, E.; Salant, A.; Banin, U. Visible Light-Induced Charge Retention and Photocatalysis with Hybrid CdSe–Au Nanodumbbells. *Nano Lett.* **2008**, *8*, 637–641.
23. Khon, E.; Mereshchenko, A.; Tarnovsky, A.; Acharya, K.; Klinkova, A.; Hewa-Kasakarage, N.; Nemitz, I.; Zamkov, M. Suppression of the Plasmon Resonance in Au/CdS Colloidal Nanocomposites. *Nano Lett.* **2011**, *11*, 1792–1799.
24. Bao, N.; Shen, L.; Takata, T.; Domen, K. Self-Templated Synthesis of Nanoporous CdS Nanostructures for Highly Efficient Photocatalytic Hydrogen Production under Visible Light. *Chem. Mater.* **2008**, *20*, 110–117.
25. Elmalem, E.; Saunders, A. E.; Costi, R.; Salant, A.; Banin, U. Growth of Photocatalytic CdSe–Pt Nanorods and Nanonets. *Adv. Mater.* **2008**, *20*, 4312–4317.
26. Berr, M.; Vaneski, A.; Susha, A. S.; Rodríguez-Fernández, J.; Döblinger, M.; Jäckel, F.; Rogach, A. L.; Feldmann, J. Colloidal CdS Nanorods Decorated with Subnanometer Sized Pt Clusters for Photocatalytic Hydrogen Generation. *J. Appl. Phys. Lett.* **2010**, *97*, 093108.
27. Amirav, L.; Alivisatos, P. A. Photocatalytic Hydrogen Production with Tunable Nanorod Heterostructures. *J. Phys. Chem. Lett.* **2010**, *1*, 1051–1054.
28. Acharya, K. P.; Khnayzer, R. S.; O'Connor, T.; Diederich, G.; Kirsanova, M.; Klinkova, A.; Roth, D.; Kinder, E.; Imboden, M.; Zamkov, M. The Role of Hole Localization in Sacrificial Hydrogen Production by Semiconductor–Metal Heterostructured Nanocrystals. *Nano Lett.* **2011**, *11*, 2919–2926.
29. Habas, S. E.; Yang, P.; Mokari, T. Selective Growth of Metal and Binary Metal Tips on CdS Nanorods. *J. Am. Chem. Soc.* **2008**, *130*, 3294–3295.
30. Kirsanova, M.; Nemchinov, A.; Hewa-Kasakarage, N. N.; Schmall, N.; Zamkov, M. Synthesis of ZnSe/CdS/ZnSe Nanobarbells Showing Photoinduced Charge Separation. *Chem. Mater.* **2009**, *21*, 4305–4309.
31. Baker, D. R.; Kamat, P. V. Tuning the Emission of CdSe Quantum Dots by Controlled Trap Enhancement. *Langmuir* **2010**, *26*, 11272–11276.
32. Peng, P.; Milliron, D. J.; Hughes, S. M.; Johnson, J. C.; Alivisatos, A. P.; Saykally, R. J. Femtosecond Spectroscopy of Carrier Relaxation Dynamics in Type II CdSe/CdTe Tetrapod Heteronanostructures. *Nano Lett.* **2005**, *5*, 1809–1813.
33. Dooley, C. J.; Dimitrov, S. D.; Fiebig, T. Ultrafast Electron Transfer Dynamics in CdSe/CdTe Donor–Acceptor Nanorods. *J. Phys. Chem. C* **2008**, *112*, 12074–12076.
34. Chuang, C. H.; Lo, S. S.; Scholes, G. D.; Burda, C. Charge Separation and Recombination in CdTe/CdSe Core/Shell Nanocrystals as a Function of Shell Coverage: Probing the Onset of the Quasi Type-II Regime. *J. Phys. Chem. Lett.* **2010**, *1*, 2530–2535.
35. Chuang, C. H.; Doane, T. L.; Lo, S. S.; Scholes, G. D.; Burda, C. Measuring Electron and Hole Transfer in Core/Shell Nanoheterostructures. *ACS Nano* **2011**, *5*, 6016–6024.
36. Rawalekar, S.; Kaniyankandy, S.; Verma, S.; Ghosh, H. N. Ultrafast Charge Carrier Relaxation and Charge Transfer Dynamics of CdTe/CdS Core–Shell Quantum Dots as Studied by Femtosecond Transient Absorption Spectroscopy. *J. Phys. Chem. C* **2010**, *114*, 1460–1466.
37. Lupo, M. G.; Sala, F. D.; Carbone, L.; Zavelani-Rossi, M.; Fiore, A.; Lüer, L.; Polli, D.; Cingolani, R.; Manna, L.; Lanzani, G. Ultrafast Electron–Hole Dynamics in Core/Shell CdSe/CdS Dot/Rod Nanocrystals. *Nano Lett.* **2008**, *8*, 4582–4587.
38. Jiang, Z. J.; Kelley, D. F. Role of Surface States in the Exciton Dynamics in CdSe Core and Core/Shell Nanorods. *J. Phys. Chem. C* **2010**, *114*, 17519–17528.
39. Hewa-Kasakarage, N. N.; El-Khoury, P. Z.; Schmall, N.; Kirsanova, M.; Nemchinov, A.; Tarnovsky, A. N.; Bezryadin, A.; Zamkov, M. The Effect of Dielectric Friction on the Rate of Charge Separation in Type II ZnSe/CdS Semiconductor Nanorods. *App. Phys. Lett.* **2009**, *94*, 133113–133115.
40. Kaniyankandy, S.; Rawalekar, S.; Verma, S.; Ghosh, H. N. Ultrafast Hole Transfer in CdSe/ZnTe Type II Core–Shell Nanostructure. *J. Phys. Chem. C* **2011**, *115*, 1428–1435.
41. Yan, Y.; Chen, G.; Van Patten, P. G. Ultrafast Exciton Dynamics in CdTe Nanocrystals and Core/Shell CdTe/CdS Nanocrystals. *J. Phys. Chem. C* **2011**, *115*, 22717–22728.
42. Khon, E.; Mereshchenko, A.; Tarnovsky, A. N.; Acharya, K.; Klinkova, A.; Hewa-Kasakarage, N. N.; Nemitz, I.; Zamkov, M. Suppression of the Plasmon Resonance in Au/CdS Colloidal Nanocomposites. *Nano Letters.* **2011**, *11*, 1792–1799.
43. Berr, M. J.; Vaneski, A.; Mauser, C.; Fischbach, S.; Susha, A. S.; Rogach, A. L.; Jäckel, F.; Feldmann, J. Delayed Photoelectron Transfer in Pt-Decorated CdS Nanorods under Hydrogen Generation Conditions. *Small.* **2012**, *8*, 291–297.
44. Wu, K.; Zhu, H.; Liu, Z.; Rodríguez-Córdoba, W.; Lian, T. Ultrafast Charge Separation and Long-Lived Charge Separated State in Photocatalytic CdS–Pt Nanorod Heterostructures. *J. Am. Chem. Soc.* **2012**, *134*, 10337–10340.
45. Schaller, R. D.; Pietryga, J. M.; Goupalov, S. V.; Petruska, M. A.; Ivanov, S. A.; Klimov, V. I. Breaking the Phonon Bottleneck in Semiconductor Nanocrystals *via* Multiphonon Emission Induced by Intrinsic Nonadiabatic Interactions. *Phys. Rev. Lett.* **2005**, *95*, 196401.
46. Klimov, V.; Hunsche, S.; Kurz, H. Biexciton Effects in Femtosecond Nonlinear Transmission of Semiconductor Quantum Dots. *Phys. Rev. B* **1994**, *50*, 8110–8113.
47. Hunsche, S.; Dekorsy, T.; Klimov, V.; Kurz, H. Ultrafast Dynamics of Carrier-Induced Absorption Changes in Highly-Excited CdSe Nanocrystals. *Appl. Phys. B: Laser Opt.* **1996**, *62*, 3–10.
48. Landolt-Boernstein. Numerical Data and Functional Relationships. In *Science and Technology*; Group III, Condensed Matter, SubVol. C; Martienssen, W., Ed.; Springer: Verlag, 1998.
49. Dinger, A.; Petillon, S.; Grün, M.; Hetterich, M.; Klingshirn, C. Conduction Band Offset of the CdS/ZnSe Heterostructure. *Semicond. Sci. Technol.* **1999**, *14*, 595–598.
50. Burda, C.; Link, S.; Mohamed, M.; El-Sayed, M. The Relaxation Pathways of CdSe Nanoparticles Monitored with Femtosecond Time-Resolution from the Visible to the IR: Assignment of the Transient Features by Carrier Quenching. *J. Phys. Chem. B* **2001**, *105*, 12286–12292.
51. Sacra, A.; Norris, D. J.; Murray, C. B.; Bawendi, M. G. Stark Spectroscopy of CdSe Nanocrystallites: The Significance of Transition Linewidths. *J. Chem. Phys.* **1995**, *103*, 5236.
52. Mokari, T.; Aharoni, A.; Popov, I.; Banin, U. Diffusion of Gold into InAs Nanocrystals. *Angew. Chem., Int. Ed.* **2006**, *118*, 8169.
53. Brown, K. A.; Wilker, M. B.; Boehm, M.; Dukovic, G.; King, P. W. Characterization of Photochemical Processes for H_2 Production by CdS Nanorod–[FeFe] Hydrogenase Complexes. *J. Am. Chem. Soc.* **2012**, *134*, 5627–5636.
54. Cozzoli, P. D.; Manna, L.; Curri, M. L.; Kudera, S.; Giannini, C.; Striccoli, M.; Agostiano, A. Shape and Phase Control of Colloidal ZnSe Nanocrystals. *Chem. Mater.* **2005**, *17*, 1296–1306.
55. Hewa-Kasakarage, N. N.; El-Khoury, P. Z.; Tarnovsky, A. N.; Kirsanova, M.; Nemitz, I.; Nemchinov, A.; Zamkov, M. Ultrafast Carrier Dynamics in Type II ZnSe/CdS/ZnSe Nanobarbells. *ACS Nano* **2010**, *4*, 1837–1844.